Chinese Journal of Physiology 53(2): 77-90, 2010
DOI: 10.4077/CJP.2010.AMK045

Review

Physiological Rhythms, Dynamical Diseases and Acupuncture

Shyang Chang

Department of Electrical Engineering, National Tsing Hua University
Hsinchu 300, Taiwan, R.O.C.

Abstract

Physiological rhythms are ubiquitous and essential to our life. They usually interact with one another and also with the outside environment. Disappearance of normal rhythms and emergence of abnormal rhythms are called dynamical diseases. In this article, we will first review the current knowledge on the genesis of physiological rhythms. Then, models of rhythmic interactions among themselves and with external stimuli will be reviewed. Particular emphasis will be placed on the methods that can diagnose abnormal rhythms. Finally, treatment of dynamical diseases will be discussed. It turns out that the models of fractional Brownian motion and fractional Gaussian noise based on dynamical systems have the potential to become biomarkers in differentiating and evaluating normal from abnormal physiological rhythms in dynamical diseases. Meanwhile, in order to explain how acupuncture works, a feasible model of meridians based on communication networks is also included.

Key Words: acupuncture, dynamical disease, fractional Brownian motion, fractional Gaussian noise, rhythmogenesis, synergic co-activation, traditional Chinese medicine

Introduction

Both simple and complex bodily rhythms are ubiquitous in physiology. Familiar examples are the rhythmic contractility of the heart, respiratory movements in lungs, peristalsis of the stomach, systole and diastole of the spleen, rhythmic movements of digestive intestines, contraction of the bladder during micturition and rhythmic co-activations of limb muscles during volitional movements (2, 3, 4, 9, 13, 14, 24, 27, 29, 30, 35, 36, 47, 55, 56). These physiological rhythms usually do not exist in isolation. Rather, they have complex interactions among themselves. For instance, cardiac and pulmonary rhythms begin interaction in the uterus; rhythmic dilatation and contraction of the stomach, the spleen and intestines are co-activated during the process of digestion; synergic contractions of the bladder and external urethral sphincter (EUS) prevail in the voiding phase of micturition; and rhythmic co-activations of coupled striated muscles exist in human elbow flexion and forearm pronation. Two typical physiological rhythms, one regular and one irregular, are presented in Figs. 1 and 2.

In addition to the multiple interactions in the internal environment, physiological rhythms may also interact with external environment. For instance, circadian rhythm can be perturbed by jet lag and the time of bright light exposure. Furthermore, the phase shifting of menstrual cycles can be accomplished by visible light stimulation (59, 60). During the interactions of multiple rhythms, health can be viewed as harmony among these rhythms, and disease discord. Therefore, the disruption of normal rhythms and emergence of abnormal rhythms are called “dynamical diseases” (37, 38). Hence, the definition of “dynamical disease” is synonymous with the abnormal condition of physiological rhythms in space and time.

In this review, we will first examine several models of rhythmogenesis that have been proposed. They include pacemaker oscillations, central pattern generators of mutual inhibition and sequential disinhibition. The pros and cons of each model of rhythmogenesis will be reviewed. As to the interactions of

Corresponding author: Dr. S. Chang, Department of Electrical Engineering, National Tsing Hua University, Hsinchu 300, Taiwan, ROC. Tel: +886-35731146, Fax: +886-35715971, E-mail: shyang@ee.nthu.edu.tw
Received: July 15, 2009; Revised: October 23, 2009; Accepted: November 10, 2009.
 ISSN : 0304-4920. http://www.cps.org.tw

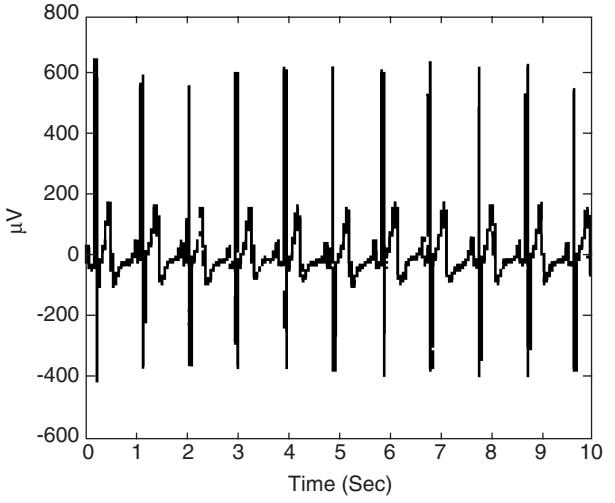

Fig. 1. Typical electrocardiograms.

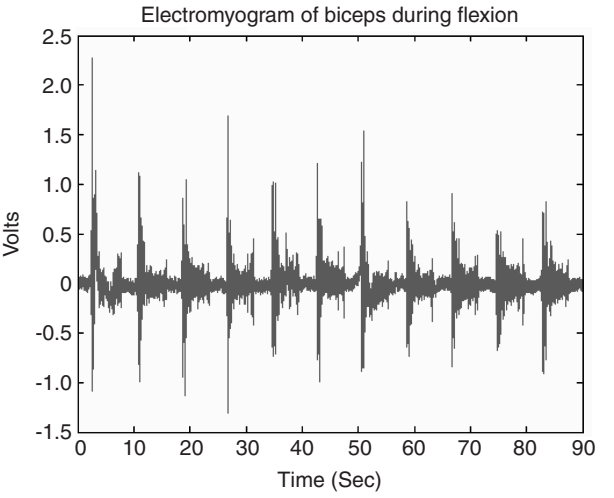

Fig. 2. Typical EMGs.

rhythms, various paradigms in terms of reciprocal inhibition, synergic co-activations and cooperative co-activations will be examined. Particular emphasis will be placed upon the detection and diagnosis of the emergence of abnormal rhythms and disappearance of normal rhythms during the interactions using fractional Brownian motion (FBM) and fractional Gaussian noise (FGN) of dynamical systems (31, 48, 49, 51). Finally, methods that can help restore normal rhythms or control pathological ones in dynamical diseases will also be reviewed.

Rhythmogenesis in Physiology

Pacemaker oscillations modeled by nonlinear differential equations played an important role in generating physiological rhythms. Hodgkin and Huxley used properties of ionic channels in the membrane of giant squid axon to construct the dynamical equations for the generation of action potentials (41). In their models, the action potentials were generated as a result of sodium and potassium ionic channels that would open and close as a result of electrical or chemical changes in an axon's intracellular and extracellular environment. The membrane currents that fluctuated according to the opening and closing of ionic channels were mainly contributed by the concentration gradients, membrane conductance and membrane capacitance. The techniques developed by these authors were adopted to studying the mechanism of cardiac rhythmogenesis. Moreover, it was believed that this type of cellular mechanism could be extended to cells that are excitable. However, the number of ionic channels of a typical cell is at least of the order 10^3 of each different type. Hence, the mathematical modeling of ionic channels for physiological systems is still a difficult task.

There are other drawbacks too. For instance, the experimentally observed discontinuous phase-resetting function could hardly be accounted for by models formulated as differential equations (38). Furthermore, the sodium and other membrane pumps in the ionic theory of action potential could suffer from insufficiency in energy to operate. Hence, an adsorption and induction hypothesis was conjectured that the action potential was actually due to the result of transient variation of the surface adoption potentials on one or both sides of the membrane (46). Consequently, there was no need of continual energy expenditure in describing the resting potential. However, the experimental tests of the propagation of electric polarizations or inductive effects along the excitable membranes were sketchy and more studies were required.

Another class of models was proposed for motor rhythms in the central pattern generators of mammals – the neural network interaction models. The cells in the network might receive tonic inputs that led to rhythms due to network interactions. Mechanisms involving mutual inhibition and sequential disinhibition had been proposed in diverse contexts (5, 38). As to the sequential disinhibition model, it was postulated that there were functionally distinct pools of neurons that received excitatory input such that the interactions within each single pool was excitatory. However, the interactions among these pools were inhibitory that the activities in the first pool tended to inhibit those of the second. Once the second pool of neurons was inhibited, the third one could then become active since it was disinhibited. This type of model had been used in the rhythmogenesis of respiration (38). However, unambiguous identification of such networks had not yet occurred. Furthermore, this type of network models would be difficult in quantitatively explain-

ing the complex interactions among different central pattern generators and their adaptations with the outside world by either single pulse perturbation or periodic stimulation.

As a matter of fact, the generation of rhythms may not be so sophisticated. It is the interaction of rhythms that can be quite complex. For instance, the strings of a violin could be either bowed or plucked to induce vibrations. The sound vibrations would last a long time if there was only minor dissipation of energy. The situation would be very similar for the simple harmonic oscillations of mechanical springs and the electromagnetic analogue of electric circuits and transmission lines. For instance, an elastic spring is usually equipped with the properties of elasticity and inertia. Once it is stretched and then released, the potential energy of elasticity will be converted to kinetic energy due to the spring inertia. If the damping is negligible, the mainspring of a self-winding watch can store energy and act for a long time. Similarly, for an electric circuit containing a condenser and an inductor, the oscillation of current can occur if the charges on the condenser are changed and then it is allowed to discharge to the inductor through a simple circuit. In addition, the current oscillation of the circuit can be propagated as a traveling wave along the transmission lines without distortion if the line parameters can satisfy the distortionless condition, *i.e.*, the ratio of capacitance to the inductance is equal to the ratio of conductance to resistance. Actually, the numerical data of a giant squid axon had shown that the distortionless condition for the propagation of action potentials along its axon could be satisfied (20). Hence, it is reasonable to assume that the rhythmic activities could be generated by chemical, mechanical or electromagnetic stimuli on the capacitive/inductive nerves of a compactum.

Interactions of Physiological Rhythms

The paradigms of interactions of physiological rhythms include reciprocal inhibition (33, 34, 44, 55, 57), synergic and cooperative co-activations (7, 12-19, 22, 23, 42). The story of inhibition began with the tetanic excitation of vagus nerve that caused a standstill of the frog's heart by the brothers of Weber in 1845 (55). It was known at that time that the heart was also supplied by fibers from the sympathetic system. The functions of these two nerve systems were thought to be opposite or antagonistic. However, one of the opponents of this view was Schiff and he contended that the inhibition was due to over-stimulation and exhaustion of these nerve fibers (55). In spite of the opposition, it is now commonly taught in schools that the sympathetic and parasympathetic systems exert an antagonistic effect upon the heart that they mutually innervate. Valentin adopted a similar idea in micturition by suggesting that the striated musculature of EUS was voluntarily relaxed while the bladder contracted (45). Since then, the antagonistic actions of autonomic innervations on the gastric secretion and digestive tracts were also vigorously studied (32, 47).

In the same vein, the volitional elbow flexion was believed to display reciprocal innervations of antagonistic muscles (57). For instance, in the flexion of the elbow joint, the triceps were thought to be relaxed and the biceps in active contraction. In other words, one muscle of an antagonistic couple was thrown out of action while the other was brought into action. This concept was referred to as reciprocal inhibition (4, 6-8, 57). Thus, it was assumed that there were two groups of neurons. Interactions within each group were excitatory, but interactions between the two were inhibitory. The motor interneurons that were thought to be responsible for the inhibition were called Renshaw cells (28, 50). However, the real functions and roles of these cells in motor control and behavior were still lacking as could be seen from the following quotes of a recent review paper (1):

'Although Renshaw cells participate in a relatively "simple" local recurrent inhibitory circuit, and much is known about their physiology and morphology, it is humbling to recognize that there is as yet no definitive functional hypothesis regarding their contributions to motor control and behavior... It has been difficult to directly test these and related hypotheses because of the lack of experimental tools to selectively anatagonize/delete/knockout Renshaw cells or monitor their behavior in freely moving non-anaesthetized animals.'

In the aforementioned *local recurrent inhibitory circuit*, it was referred to the synaptic transmission between nerve cells. It was in 1892 that Langley (50) first proposed the idea that synaptic transmission in the autonomic ganglia of mammals was chemical. Eccles and his colleagues then studied the end-plate potentials in muscles and the synaptic potentials in nerve cells to conclude that both presynaptic and postsynaptic inhibitory permeability changes were required to account for inhibition (50). Since then, the synaptic excitatory and inhibitory concepts had been extensively studied and were even extended to the higher functions of human brain in terms of spike-timing-dependent synaptic plasticity (21). However, the main drawbacks in proposing the presynaptic and postsynaptic inhibition for synaptic plasticity were twofold. First, the time scales of inhibitory potentials and synaptic efficacy were obtained in terms of *milliseconds* or tens of *milliseconds*. To use the results of time span in milliseconds for explaining higher functions of learning and memory would not

be very convincing. For instance, the sense of *déjà vu* that has to do with long-term memory certainly has a time span much longer than *milliseconds* or *minutes*. Secondly, the experiments performed would usually need stronger stimuli to produce inhibitory responses while weaker stimuli often resulted in excitation (50). Hence, it would be curious to ask if the inhibitory hyperpolarization was actually derived from over-stimulation and exhaustion of these synapses as suggested by Schiff more than a century ago. This issue can definitely be resolved if direct proofs of inhibitory response of synaptic plasticity in freely moving non-anaesthetized animals or humans are provided.

Recently, based on the studies of micturition and storage of urine in Wistar rats (12, 15, 17-19), elbow flexion in humans and the forearm pronation for patients of radial nerve palsy, the so-called reciprocal inhibitions were not observed (13, 14). Instead, synergic and cooperative co-activation in normal physiological rhythms was found. For instance, during the voiding phase of micturition, the rhythms of the detrusor and EUS of Wistar rats were synchronized around 7 Hz and their intensities as functions of time were temporally correlated to facilitate the concerted voiding process (15). On the other hand, for the spinal cord-injured rats, either the temporal strength or its underlying synchronization of rhythms was impaired, weakened or completely vanished depending on the degrees of injury (15). As to the characterization of urine storage, it was also found that the EUS of Wistar rats was not activated. It was the cooperative sympathetic and parasympathetic nerve activities of the bladder in female Wistar rats that were dominant (12).

As to the human forearm pronation, the surface electromyograms (EMG) included the short and long heads of the biceps brachii (BBSH, BBLH), the brachialis (B), the lateral head of the triceps brachii (TBLTH), brachioradialis (BR) and pronator teres (PT) were recorded during action. Experimental results of the healthy group indicated that the surface EMGs of all muscles were temporally synchronized in frequencies with persistent intensities (14). Hence, all involved muscle groups were in synergic co-activation. As to the group of patients of radial nerve palsy, results indicated that the EMG might have bursting activities, but either the synchronized significant frequencies were lacking or the intensities as indicated from their fractal dimensions were not persistent. The same situation was found for the elbow flexion case (13).

The theoretical foundation for the aforementioned results was based on the models of FGN and FBM (49). They were proposed to model interacting physiological rhythms from neural or muscular systems (12-19). The rationale behind these models was motivated by the theory of dynamical systems. They could be described as follows and more detailed descriptions could be found in (43). In general, a dynamical system is defined as the triple (M, μ, ϕ_t), where M is a compact manifold, μ a measure on M, and $\phi_t : M \to M$ a one parameter group of continuous, measure-preserving transformation. The parameter t could be a real number or an integer. When it is an integer, ϕ_t is generated by a measure-preserving transformation $\phi = \phi_1$. The discrete dynamical system can be denoted as (M, μ, ϕ). A simple example for such a discrete dynamical system is to let M be the torus $\{(x, y)(\text{mod}1)$, the measure $\mu = dxdy$, and $\phi(x, y) = (2x + y, x + y)(\text{mode}1)$. This Anosov dynamical system on the compact torus is structurally stable, ergodic, mixing, and has dense periodic orbits (43). Other transformations are also possible. For instance, if we set $\phi(x, y) = (x + \omega_1, y + \omega_2)(\text{mode}1)$, the orbits of ϕ would be periodic or dense depending on whether the ratio of ω_1/ω_2 is rational or not. The aforementioned variables x and y could represent the phases of the rhythms in sympathetic and parasympathetic nervous systems, or those in the interaction of cardiac and pulmonary rhythms in physiological applications. If the torus is taken to be our phase space of interacting rhythms, the set $\{e^{2\pi i(px + qy)}\}$ where p and q are integers is an orthonormal basis of $L^2(M, \mu)$. Each individual physiological signal can be viewed as the projection of $L^2(M, \mu)$ functions on its proper subspace. In physiological applications, when many neural or muscle fibers are superposed, the rhythms can be defined formally as an infinite series of oscillations with random amplitudes $\sum_{n=-\infty}^{\infty} \xi_n e^{2\pi inx}$ where $\{\xi_n\}$ is a sequence of independent and identically distributed standard Gaussian random variables. Notice that this infinite sum is not convergent, but if we integrate it with respect to x from 0 to t as the cumulative effects of time, the integral $B(t) = \int_0^t \sum_{n=-\infty}^{\infty} \xi_n e^{2\pi inx} dx$ will converge almost surely and in the L^2 sense. It turns out that this integral is the rigorous mathematical construction of the Brownian movement proposed in the 1930s by Norbert Wiener (51) and it is used later in his studies on brain waves. Hence, the Brownian motion is a good model for the cumulative effects of many neural or muscle fibers. It is worth noting that the increments of the Brownian motion are stationary and independent (26). Yet, empirical studies often suggested the existence of long-term dependence between samples. Thus, B. Mandelbrot proposed in 1968 the FBM with correlated increments for practical applications. Detailed formulations of FBM and FGN are defined in (49) and are not repeated here.

In applying the aforementioned concepts to physiological rhythms, the surface EMG signals could be modeled as FBM and the sampled version of the surface EMG signals as discrete-time fractional Brownian motion (DFBM) (13, 14, 16). In DFBM, there is an important Hurst parameter H. The fractal dimension (FD), D, is related to the parameter H by $D = 2 - H$. This H could also be derived from the DFGN (13, 14, 16). By using the FD and spectral frequencies, the concepts of *synergic* and *cooperative co-activations* can be defined. Here, the descriptive term of describing coupled neural or muscle groups being "*synchronized*" is used to denote that they all have the *same frequencies* during action. The term "*synergic*" is used to denote that they have both the *same frequencies* and the persistent signal *intensities* in their noise-like waveforms. The term "*cooperative*" is used to denote that they may have *different frequencies* but with persistent signal *intensities* (12-14). The importance of having the persistent intensities is equivalent to being co-active with strength in physiological functions. Notice that the advantage of using simple dynamical systems on compact manifolds is that they can give rise to FBM and FGN without using complicated ordinary or partial differential equations. As a result, these models would be more plausible in physiological applications.

Detection and Diagnosis in Dynamical Diseases

In dynamical diseases, both regular and irregular periodicities are possible. For instance, the electrocardiogram (ECG) of heart rate could still be regular and the EMG irregular. Hence, it is usually hard to detect and diagnose abnormal rhythms. The reasons are threefold. First, normal fluctuations in physiology could be regular or irregular. There is no clear-cut measure to tell the difference. Secondly, *in vivo* normal rhythms are difficult to obtain for different physiological tissues, organs and systems. Thirdly, no good parameters are proposed to characterize the rhythms. However, if we can identify for sure the ranges of normality with robust parameters, then the abnormal conditions can be positively identified. The advantages of dynamical system approaches using FBM and FGN are that we can use their FDs (15, 16, 39, 40) and spectral frequencies to distinguish normal physiological rhythms from the abnormal ones with minimal assumptions. For instance, the signal intensities of physiological rhythms in EMGs are usually low and are buried in random-like noise. We can eliminate the effects of noise and obtain the "signal intensity" from the covariance function. The covariance function of FBM can be computed as $\langle (B_H(t))^2 \rangle \sim t^{2H}$. Here the term $\langle (B_H(t))^2 \rangle$ is equivalent to the average "signal intensity" and it is proportional to H and inversely to the corresponding $D = 2 - H$. For Brownian motion, the value of H is 0.5 and D = 1.5. It can reflect the state that the coupled muscle groups are independent and are not recruited together. If H is greater than 0.5, *i.e.*, $1 < D < 1.5$, the interpretation is that the integrated effects of muscle groups can be categorized as positively correlated or persistent as in (20, 35). For example, in Figs. 3a-3e, the drastic drops of FDs from green to blue color code imply that the coupled muscle groups exhibit strong and persistent signal intensities. If D is between 1.5 and 2, the corresponding effect can be interpreted as negatively correlated or anti-persistent (20, 35). Notice that the covariance function of DFGN is also proportional to H. Consequently, D can be used as an indicator of the persistence of "signal intensity" in the DFBM and DFGN models.

A second important indicator is the spectral frequency. In order to obtain these two indicators at the same time, a novel algorithm using spectral distribution function *via* DFGN was proposed in (16). The basic idea in using these two parameters was that if the spectral frequencies were not observed, or the intensities of coupling were not strong enough as compared to those of the normal ones, one could then conclude that the physiological rhythms were not normal.

Here, two examples would be used to illustrate the aforementioned ideas (13, 17). The first one is to use the two indicators in characterizing normal rhythms of EMG in humans, and the second one is to characterize the abnormal rhythms of spinal cord-injured (SCI) Wistar rats against normal ones during micturition. In Fig. 3, surface EMG activities, temporal FDs and spectra of five different brachial muscles of a right upper arm during flexion are shown. The activities of surface EMG are in dark color and temporal FDs in color codes for muscles of (a) BBSH, (b) BBLH, (c) B, (d) TBLTH, and (e) the long head of the triceps brachii (TBLH), respectively. The corresponding spectral frequencies for these muscles are presented from (g) to (k), respectively. The elbow flexion angle in vertical axis from an electrogoniometer is presented in (f). It is clear from these illustrations that the temporal coherent FDs and synchronized spectral frequencies could characterize the synergic activities of muscles.

The second case is the co-activations during micturition of intact and SCI rats. In Fig. 4, the normal rhythms of the intact rat could be differentiated *via* FD and spectral frequencies from the abnormal ones of SCI rats as shown in Fig. 5. In Fig. 4(a), from the alteration of the EMG and cystometrogram (CMG), the voiding phase was located during 17 to 23 sec. The maximal value of amplitudes would be denoted by Cmax and it was 0.12 in normalized unit (n.u.) as

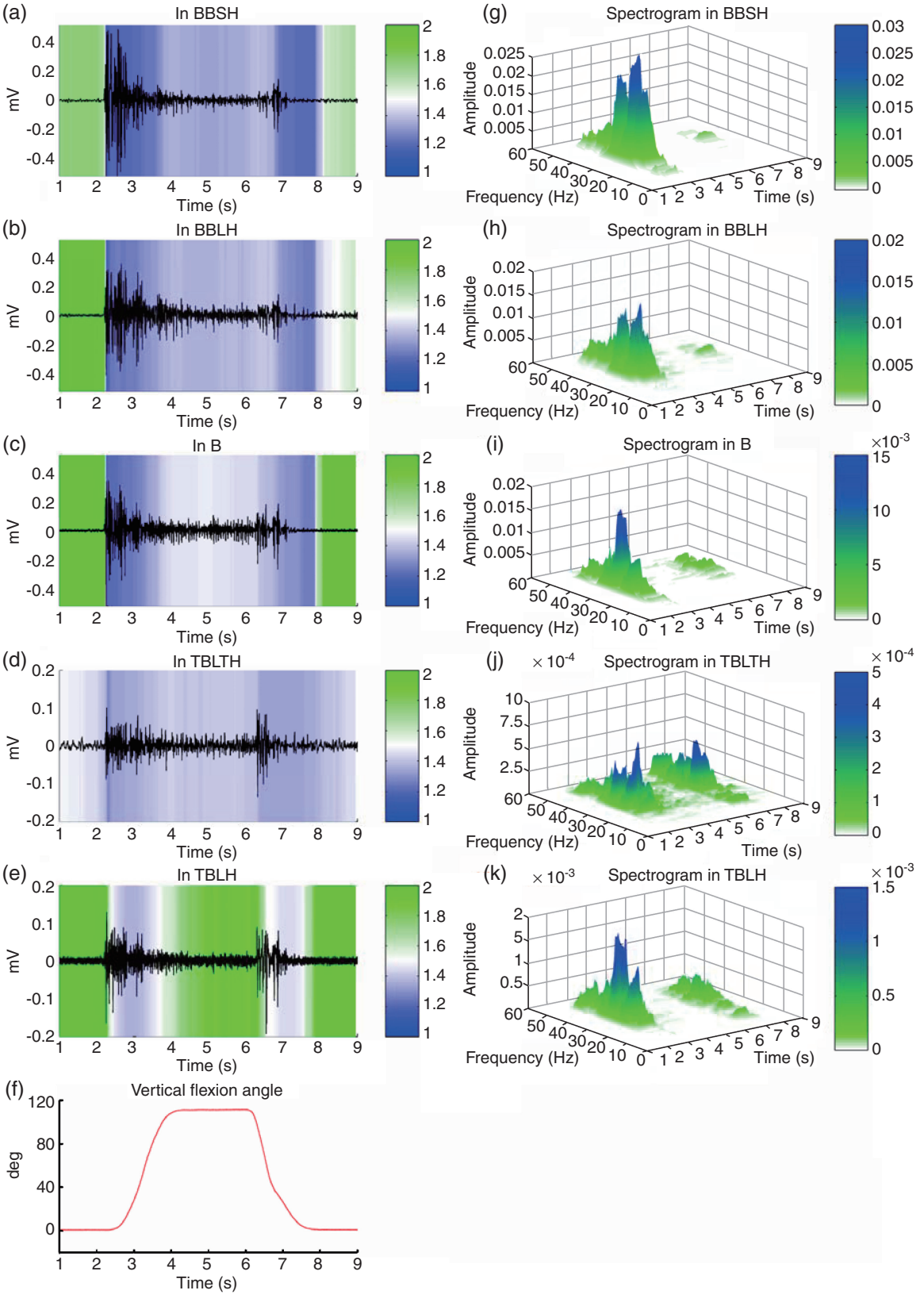

Fig. 3. Normal surface EMG activities, temporal FDs and spectrograms of five different brachial muscles of a right upper arm during flexion. The activities of surface EMG are in dark color and temporal FDs in color codes for muscles of BBSH (a), BBLH (b), B (c), TBLTH (d) and TBLH (e), respectively. The corresponding spectrograms for these muscles are presented from (g) to (k), respectively. The elbow flexion angle in vertical axis from an electrogoniometer is presented in (f). The metronome beep at 2 s to instruct the subject to flex and at 6 s to instruct the subject to extend.

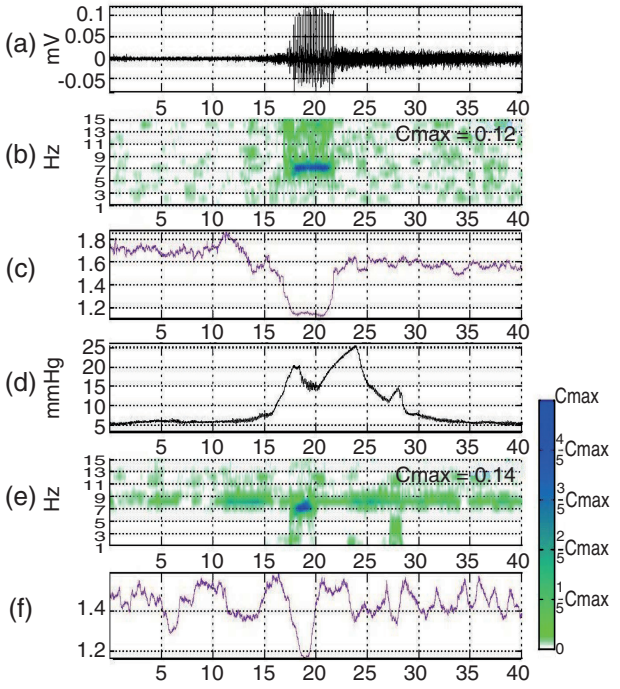

Fig. 4. Time series, spectral frequencies and FDs of one complete contraction of a normal rat. (a) 40-second EMG time series of the intact rat; (b) the spectral frequencies of EMG for EUS; (c) the FDs of the EMG for EUS; (d) 40-second CMG time series of the intact rat; (e) the spectral frequencies of CMG; (f) the FDs of the CMG.

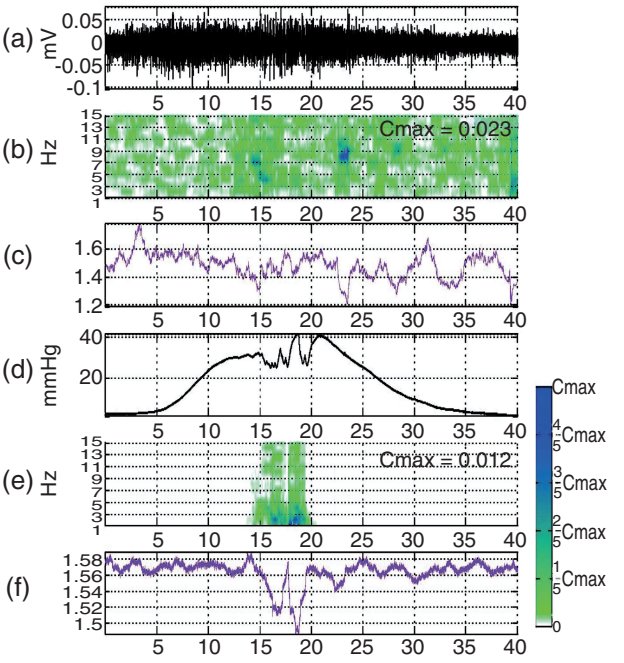

Fig. 5. Time series, spectral frequencies and FDs of one complete contraction of an SCI rat. (a) 40-second EMG time series of the SCI rat; (b) the spectral frequencies of EMG for EUS; (c) the FDs of the EMG for EUS; (d) 40-second CMG time series of the SCI rat; (e) the spectral frequencies of CMG; (f) the FDs of the CMG.

shown in Fig. 4(b); the Cmax of Fig. 4(e) was 0.14 n.u. The significant frequency component of EMG was noticeable around 7 Hz with the maximal magnitude 0.12 n.u. The significant frequency component of CMG was also around 7 Hz with the maximal magnitude 0.14 n.u. In Fig. 4(c), the drop of fractal dimension for EMG fell around 17 to 22 sec and was about 1.15 during this period. In Fig. 4(f), the drop of fractal dimension for CMG was also below 1.2 around 18 to 20 sec. Once the normal physiological rhythms were established, the abnormal rhythms of the EMG and CMG of SCI rats could be identified. In Fig. 5(a), from the alteration of the EMG and CMG, the voiding phase was located roughly between 15 sec to 20 sec. The Cmax of Fig. 5(b) was 0.023 n.u.; the Cmax of Fig. 5(e) was 0.012 n.u. No significant frequency components of EMG and CMG were noticed in these two subplots. In Fig. 5(c), the local drop of fractal dimension for EMG was minor and not conformable with that for CMG. Hence, once the normal physiological rhythms are established as in Fig. 4, the abnormal rhythms of the EMG and CMG of SCI rats in Fig. 5 could be identified.

Treatments in Dynamical Diseases

It is well-known in clinical practices that drug therapy can be used to treat various kinds of dynamical diseases. In order to evaluate its performance, objective measures have to be invoked. As mentioned in the previous section, the dynamical disease associated with normal and abnormal physiological conditions involve both irregular and regular periodicities. Hence, the effects of drugs or any treatment can be proved more effective only if the physiological conditions can be restored much closer to the normal states. The effects of drugs could be very complicated as mentioned in (52): responses to the dosage schedule of L-DOPA in treating *encephalitis lethargica* were very erratic. They would fluctuate not only hourly, but daily, weekly and monthly. Such long-term fluctuations and periodicities were also commonly seen in migraine, epilepsy and Parkinsonism (52-54). One particular interesting means of therapy using music has also been surveyed in (54). It is believed that the FDs and spectral frequencies would be helpful in the evaluation and prognosis of dynamical disease treatment. Two interesting cases are reviewed as follows (10, 11, 17).

The first case was the administration of drugs for improving the micturition function of SCI Wistar rats. The normal and abnormal conditions of the bladder and EUS were indicated in Figs. 4 and 5. The drugs resiniferatoxin (RTX) and capsaicin were used

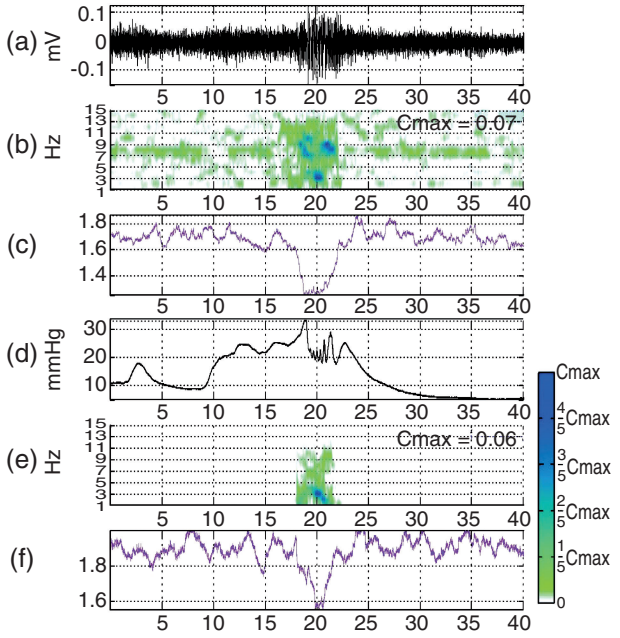

Fig. 6. Time series, spectral frequencies and FDs of one complete contraction of an SCI rat under RTX treatment. (a) 40-second EMG time series of the treated rat; (b) the spectral frequencies of EMG for EUS; (c) the FDs of the EMG for EUS; (d) 40-second CMG time series of the treated rat; (e) the spectral frequencies of CMG; (f) the FDs of the CMG.

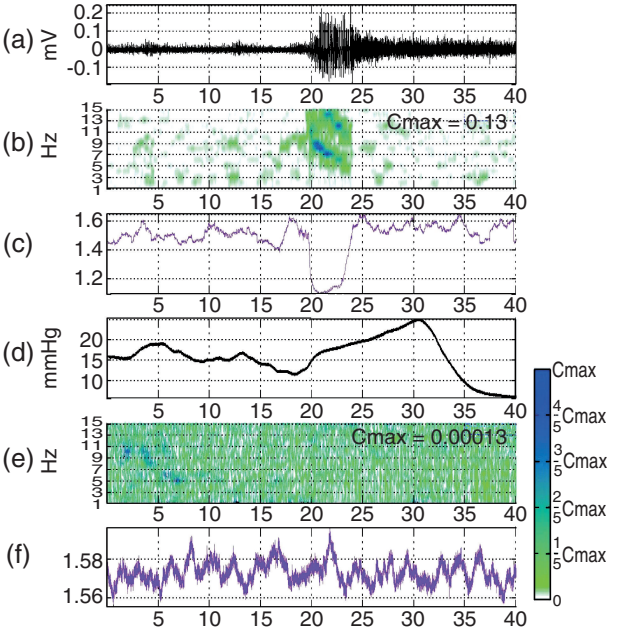

Fig. 7. Time series, spectral frequencies and FDs of one complete contraction of an SCI rat under capsaicin treatment. (a) 40-second EMG time series of the treated rat; (b) the spectral frequencies of EMG for EUS; (c) the FDs of the EMG for EUS; (d) 40-second CMG time series of the treated rat; (e) the spectral frequencies of CMG; (f) the FDs of the CMG.

to improve the micturition functions for these SCI rats. The procedures were as indicated in (17). The results are illustrated in Figs. 6 and 7. The EMG and CMG of the EUS and bladder of a SCI Wistar rat under the treatment of RTX are demonstrated in Fig. 6. In Fig. 6(a), the bursting electrical signals between 18 to 23 sec were during the voiding phase. In Fig. 6(d), the CMG showed the alteration of the bladder pressure. The Cmax in Fig. 6(b) was 0.07 n.u. and the Cmax in Fig. 6(e) was 0.06 n.u. Both subplots had synchronized frequencies around 3 Hz with rather small amplitudes as compared to 0.12 and 0.14 n.u. in Fig. 4(b) and 4(e). In Figs. 6(c) and 6(f), the FDs for EMG and CMG both fell in temporal coherence during 18 to 23 sec. However, the FDs of CMG were not smaller than 1.5 as compared to that of the intact rats in Fig. 4(f). Hence, we can see that the RTX rat has "weak" synergy during voiding due to the "weak" synchronization of rhythms and "weak" coherence of FDs.

Fig. 7 demonstrates the EMG of EUS and CMG of bladder of a SCI Wistar rat under the treatment of capsaicin. In Fig. 7(a), the bursting electrical signals between 20 to 25 sec were during the voiding phase. In Fig. 7(d), the CMG of the bladder pressure was not very clear in identifying the period of voiding. The Cmax in Fig. 7(b) was 0.13 n.u. and the Cmax in Fig. 7(e) was 0.00013 n.u. Both subplots did not have synchronized frequencies anymore. In Fig. 7(c), the FDs for EMG fell below 1.5 indicating strong oscillations. However, in Fig. 7(f), the FDs of CMG did not have any temporal coherence with those of the EMG. Hence, we could contend that the rat under capsaicin treatment was less effective as compared to the treatment of RTX since the latter had "weak" synergy during voiding while the former had not. This conclusion was later confirmed by examining the residual volume of urine in the bladders of the SCI rats (17). It is believed that this type of functional evaluation can also be applied to efficacy studies of Chinese medicinal herbs.

Another interesting application of the dynamical system approach on spatial and temporal changes of blood pressure, heart rate variability and encephalograms (EEGs) was *via* the acupuncture at Neiguan (PC 6) (10, 11). Fig. 8(a) is the typical radial arterial pulse wave that would correspond to the arterial blood pressures at the root of aorta. For instance; the magnitude of percussion wave, denoted by P, of radial artery was proportional to systolic pressure and the base point A was proportional to diastolic pressure at the root of aorta. The average of P and A, *i.e.*, (P+A)/2, was then proportional to mean blood pressure. As to the dicrotic notch, or valley V in the pulse wave, it

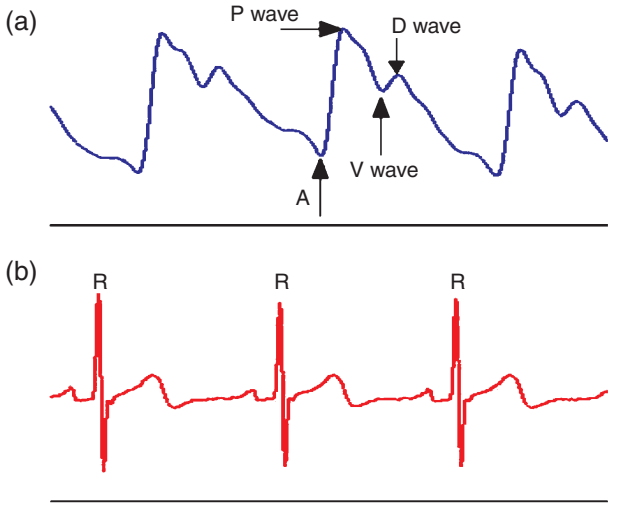

Fig. 8. Radial arterial pulse wave and ECG. (a) the typical pulse wave marked with A, P, V, D where A stands for a base point, P the percussion wave, V the valley, and D the dicrotic wave; (b) the ECG and its R peak.

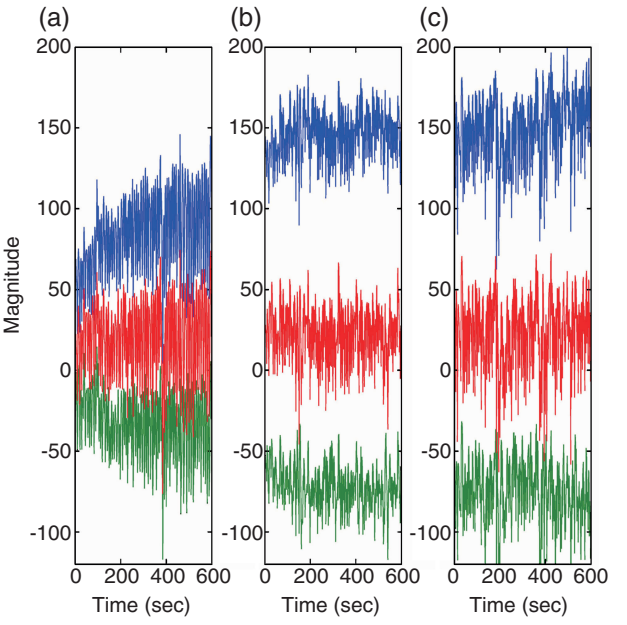

Fig. 9. The increase of magnitudes in the radial arterial pulse: amplitudes of base point A coded in green, dicrotic notch V in red, percussion wave P in blue. (a) before (b) during and (c) after manual acupuncture at PC 6.

was believed to be influenced by the peripheral resistance and compliance of local arterial tree. In the mean time, the ECG data would also be recorded to analyze the heart rate variability (HRV) that was related to the autonomic nervous system (ANS). A typical ECG diagram is illustrated in Fig. 8(b). Fig. 9 illustrates the exemplary sequences of pulse pressure magnitudes before, during and after manual acupuncture at PC 6. In these figures, the A values are coded in green, V values in red and P values in blue. The mean pulse pressures (P+A)/2 was elevated in this case. The next task was to find out the roles played by ANS. In Fig. 10, the time-frequency analyses of HRV before, during and after manual acupuncture for this typical experiment are illustrated. The spectra exhibited changes of ANS due to acupuncture stimulation. In particular, spectral frequencies of the low frequency range almost disappeared after acupuncture at the point of PC 6. Furthermore, the frequencies became more concentrated and synchronized in the very low frequency range during and after acupuncture even though the powers as indicated by the color intensities were about the same. Hence, we were sure that the peripheral ANS was involved in the changes of HRV and blood pressures. However, the ratio of power in high frequency to that in low frequency was not able to distinguish sympathetic from parasympathetic activities (11).

In order to study possible changes that occurred in the central nervous system (CNS), the field electric potentials of 12-channel EEGs were also recorded simultaneously. The spatial and temporal colored images under manual acupuncture are displayed in Figs. 11 and 12 using the EEGLAB program (25). In

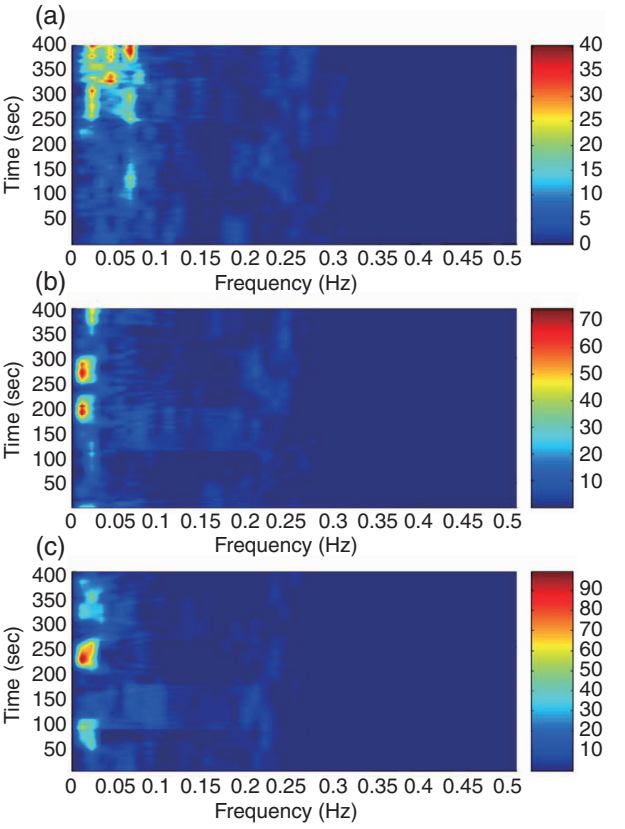

Fig. 10. Time-frequency analysis of HRV for the experiment in Fig. 9: (a) before (b) during, and (c) after manual acupuncture at PC 6. The color codes with magnitudes are on the right hand side of each part.

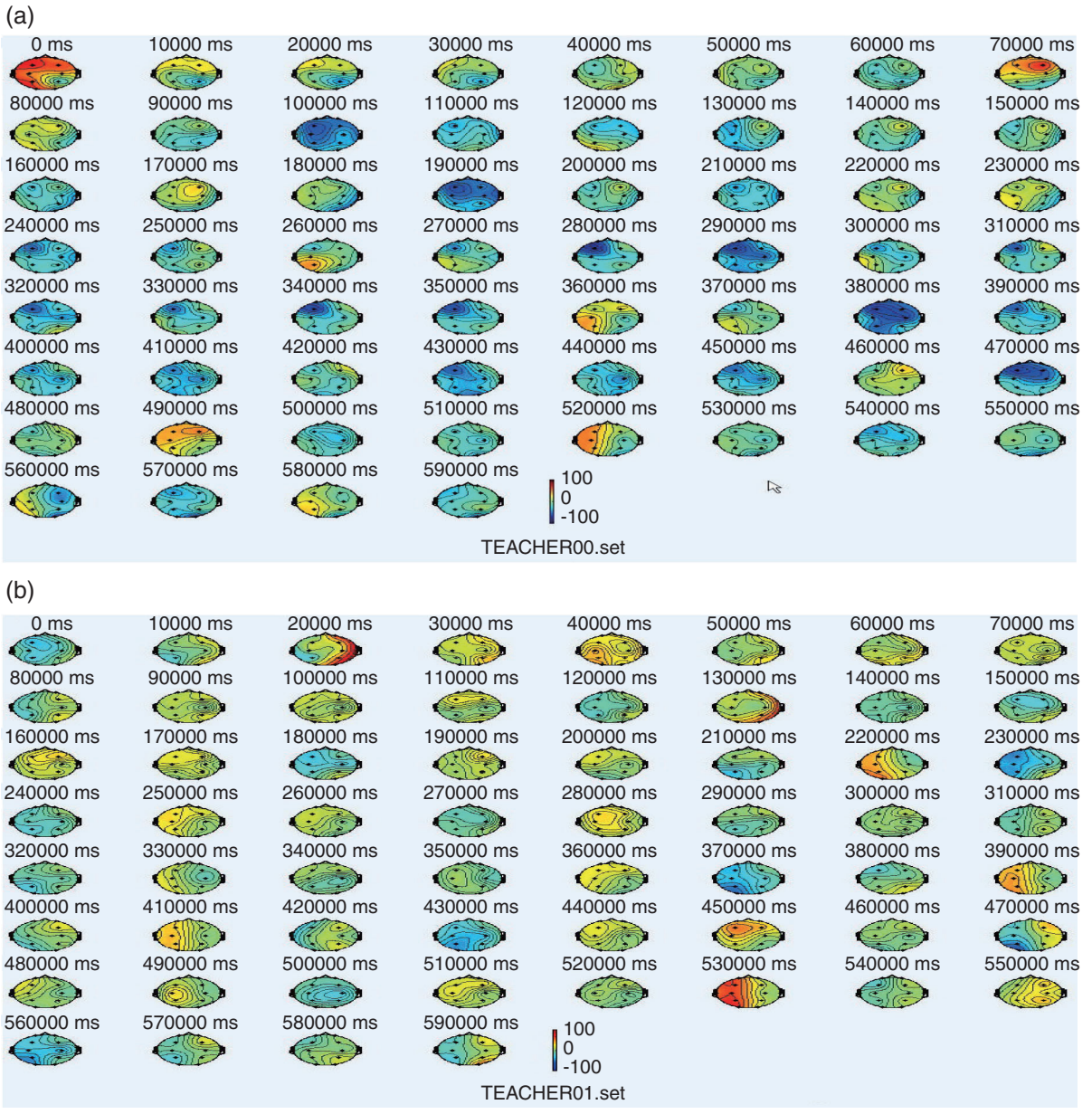

Fig. 11. Spatial powers of the 12-channel EEG for the same experiment are plotted every 10 sec for 10 min (a) before and (b) during acupuncture. The graph is similar after acupuncture and is omitted here.

Fig. 11, the spatial distributions of signal power for 12 channels before and after acupuncture are displayed. In Fig. 11(a), the average power was bluer in color which indicated that the power was relatively lower before acupuncture at PC 6. In Fig. 11(b), the average power was yellower in color which indicated that the power was relatively higher after acupuncture. In addition to the spatial changes, the EEGLAB program could also be used to plot the temporal changes of the 12 channels in Fig. 12. One could notice that the peaks in the alpha band for all 12 channels were erratic before the acupuncture, but almost all were synchronized during manual acupuncture and even completely synchronized after acupuncture. The frequencies of 12 channels were quite varied with a mean value of 8.300 Hz and a standard deviation of 0.176 Hz in the alpha band before manual acupuncture. During acupuncture, the frequencies of 12 channels were almost all synchronized at 8.202 Hz with rather smaller standard deviation of 0.081 Hz. Finally, after manual acupuncture, the frequencies were all synchronized at 8.008 Hz with a very small standard deviation of 2.03E-07 Hz.

By combining the results of ANS and CNS from Figs. 9-12, it is clear that the rhythmic changes

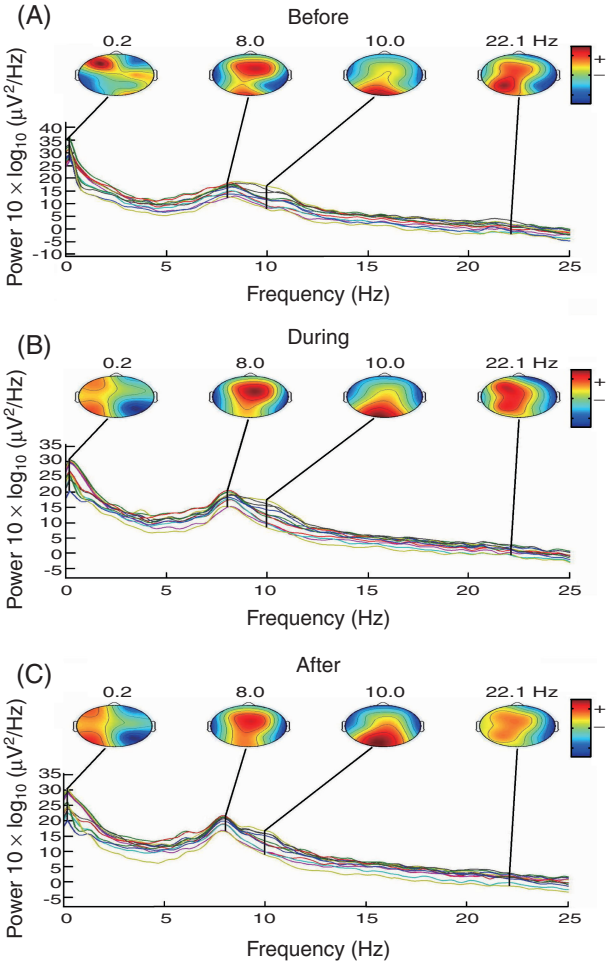

Fig. 12. The plots of the 12-channel brain maps and temporal spectra for the same experiment *via* EEGLAB software. In the alpha band, brain waves are synchronized during and after acupuncture.

occurred almost instantly in a spatial-temporal fashion. The ANS activities of the heart were exhibited in the very low frequency band (~0.2 Hz) and alpha band (8 ~ 12 Hz) of the CNS as indicated from the EEGs. The lower frequency band might have to do with the parasympathetic system and the higher alpha band with the sympathetic system. The exact interrelationship is certainly worth studying in the future. Another important point provided by this experiment was that both the synchronization of central EEGs and peripheral blood pressure changes with associated HRV were exhibited almost instantly after De Qi which took only about 15 to 30 sec. Figs. 9-12 indicate such a dramatic rhythmic change within a very short time span. This experimental result has indicated that the afferent somatosensory input near the wrist can initiate neural response of the whole brain not just restricted to the somatosensory cortex. Consequently, the brain is more likely to be holographic rather than modularly organized. In addition, one should be

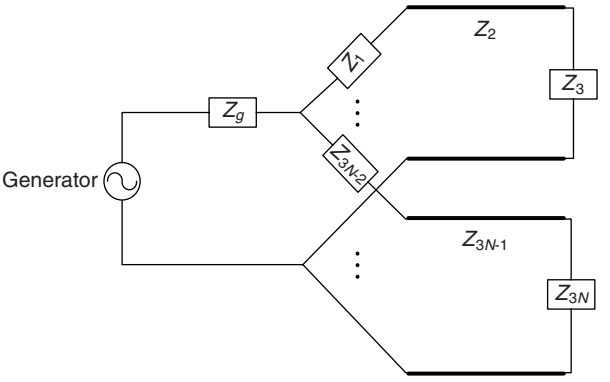

Fig. 13. A tentative model of meridians in traditional Chinese medicine.

curious to find out if it is possible to have a feasible model that can explain how the ancient Chinese acupuncture works.

Fig. 13 is such a feasible model of meridians based on the notion used in communication networks. By means of it, a plausible explanation on how acupuncture works can be given. In this figure, the meridians are characterized by transmission line impedance values Z_2, ... Z_{3n-1} for n = 1, 2, ..., N. Here N stands for the number of primary meridians and is equal to 12 in traditional Chinese medicine (TCM). According to TCM, in addition to the 12 primary meridians, there are other miscellaneous meridians that connect altogether to form a reticular system. For simplicity, the other meridians are not drawn here. The rationale for using cable theory here in modeling meridians is derived from embryogenesis. It is well-known in organogenesis that different systems of the entire organism develop simultaneously (58). They also interact and modify each other. For instance, the central and peripheral nervous systems are formed by the neural ectoderm. In the mean time, the nerve is often associated with an artery and two satellite veins under a connective tissue sheath to form a neurovascular bundle (58). The function of a meridian corresponds roughly to that of the neurovascular bundle and can be characterized by its impedance. In TCM, the meridians have the capability to control and regulate their corresponding organs. In the figure, the visceral organs that are related to the particular meridians are characterized by load impedance values Z_3, ...Z_{3n}, for n = 1, 2, ..., N. Finally, Z_1, ...Z_{3n-2}, for n = 1, 2, ..., N are used to represent proper impedance matching so that each visceral organ and its corresponding meridian will derive a proper ratio of power from either the internal or external generator of physiological rhythms with generator impedance Z_g.

In case of malfunctioning of any specific organ, the load impedance characterizing its status may

increase and it will mismatch the impedance of its corresponding meridian. As a result, the normal neurovascular flow will be partially reflected back from the needed organ in the network. For instance, the pericardial meridian that is associated with the functions of the pericardium runs down inside the arm. The cardiac tamponade can reduce cardiac output and patients may develop hypotension and circulatory collapse (58). This condition can be characterized by an increase of impedance in the pericardium, say Z_3 as in Fig. 13. Consequently, a portion of traveling waves of neurovascular flow to the pericardium will be reflected back due to the mismatch of impedance values between Z_2 and Z_3, *i.e.*, $Z_2 \neq Z_3$ in this case. If we use manual acupuncture at PC 6 along the pericardial meridian, the current of injury derived from the insertion of the needle will reduce the transmission line capacitance yet without changing too much of its longitudinal inductance of the neurovascular bundle (20). As is well known in the theory of communication networks, for an almost lossless transmission line, the impedance is roughly proportional to the square root of inductance to capacitance. Hence, after the control input of acupuncture at PC 6, the impedance of the pericardial meridian Z_2 will now be increased and possibly matched with the new Z_3 of the malfunctioned pericardium. The outcome is that there is no partial reflection and standing wave of the flow. The normal neurovascular flow to the pericardium will be resumed and the normal cardiac output and blood pressure can possibly be restored. The blood pressure variations during this whole process will be very similar to the ones presented in Fig. 9. Similar reasoning can be applied to explain the effect of pain relief *via* acupuncture. For example, the power of electric potential in Fig. 11(b) is higher than that of Fig. 11(a) after acupuncture. The impedance of the brain is now mismatched with that of the afferent pathway; hence the afferent pain signals are partially reflected back. As a result, pain relief can be achieved. It is plausible to conjecture that the mechanism of acupuncture is basically through this type of impedance matching/mismatching of meridians with its associated organs. Certainly, further studies will be required to validate these claims.

Finally, it is worth noting that the aforementioned meridian model is based on the cable theory and communication network. The mechanism of acupuncture is then explained by the concepts of impedance matching and traveling waves *via* control input at specific sites of such a network. So far, it is not easy to find a feasible model based on synaptic connections with billions of neurons. The reason is mainly due to an astronomical number of neurons and synapses. It is well known that the number of neurons in the brain is close to 100 billion. Each cortical neuron integrates information from perhaps hundreds of nearby cells and each neuron has been estimated to receive about tens of thousands of synapses. Hence, there are many billions of hierarchical neurons and synapses being active in the brain. On the one hand, if one wants to use a *parallel* model to describe the synchronization of neurons *via* synaptic transmission, the spatial integration of neurotransmitter release from these many delayed synapses will definitely make surface EEG look more like noise instead of synchronized rhythms. On the other hand, if one wants to use a *serial* model to describe the synaptic transmission, the spatial integration of neurotransmitter releases from these synapses will take days instead of seconds to achieve synchronized oscillations. However, the aforementioned model can be used to explain the synchronization of brain waves by invoking the frequency locking of oscillations in reticular networks *via* feedback mechanisms. The mechanism is very similar to the synchronization of lasers in synergetics, and that of the EUS and bladder in micturition.

Conclusions

So far, progress and development of dynamical diseases have been slow. Two key factors are: 1) difficulty in collecting long-term reliable data, and 2) the lack of simple analytic tools. In this review, we have examined several models that have been proposed in basic researches and medical treatments. Some of the prevailing models have defied simple interpretations and lack the capability of diagnosing and evaluating dynamical diseases. Yet, the recently proposed FGN and FBM models have been more intuitive and easy to apply. They have been successfully applied to the detection, diagnosis and evaluation of normal and pathological rhythms in certain cases of dynamical diseases. For instance, both the effects of drug therapy and acupuncture in dealing with physiological rhythms have been examined. In order to give a plausible explanation on how acupuncture works, a feasible model of meridians has been included in this review. It is believed that this will promote our understanding in dealing with dynamical diseases.

Acknowledgments

This work was supported in part under the grant number NSC 98-2221-E-007-066 of National Science Council, Taiwan, ROC.

References

1. Alvarez, F.J. and Fyffe, R.E.W. The continuing case for the

Renshaw cell. *J. Physiol.* 584: 31-45, 2007.
2. Barrington, F.J.F. The component reflexes of micturition in the cat. *Brain* 54: 177-188, 1931.
3. Barrington, F.J.F. The nervous mechanism of micturition. *Quart. J. Exp. Physiol*. 8: 33-71, 1914.
4. Breteler, M.D.K., Simura, K.J. and Flanders, M. Timing of muscle activation in a hand movement sequence. *Cerebral Cortex* 17: 803-815, 2007.
5. Brown, T.G. On the nature of the fundamental activity of the nervous centres; together with an analysis of the conditioning of rhythmic activity in progression, and a theory of the evolution of function in the nervous system. *J. Physiol*. 48: 18-46, 1914.
6. Buchanan, T.S., Rovai, G.P. and Rymer, W.Z. Strategies for muscle activation during isometric torque generation at the human elbow. *J. Neurophysiol.* 62: 1201-1212, 1989.
7. Busse, M.E., Wiles, C.M. and Deursen, R.W.M.V. Muscle co-activation in neurological conditions. *Physical. Therapy Rev*. 10: 247-252, 2005.
8. Caldwell, G.E., Jamison, J.C. and Lee, S. Amplitude and frequency measures of surface electromyography during dual task elbow torque production. *Eur. J. Appl. Physiol. Occup. Physiol*. 66: 349-356, 1993.
9. Chancellor, M.B. and Yoshimura, N. Physiology and pharmacology of the bladder and urethra. In: Campbell's Urology, 8th ed., edited by Walsh, P.C. Philadelphia, PA: Saunders, 2002, pp. 831-886.
10. Chang, S., Chang, Z.G., Li, S.J., Chiang, M.J., Ma, C.M., Cheng, H.Y. and Hsieh, S.H. Effects of acupuncture at Neiguan (PC 6) on electroencephalogram. *Chinese J. Physiol.* 52: 1-7, 2009.
11. Chang, S., Chao, W.L., Chiang, M.J., Li, S.J., Lu, Y.T., Ma, C.M., Cheng, H.Y. and Hsieh, S.H. Effects of acupuncture at Neiguan (PC 6) of the pericardial meridian on blood pressure and heart rate variability. *Chinese J. Physiol*. 51: 167-177, 2008.
12. Chang, S., Chiang, M.J., Li, S.J., Hu, S.J., Cheng, H.Y., Hsieh, S.H. and Cheng, C.L. The cooperative phenomenon of autonomic nervous system in urine storage. *Chinese J. Physiol*. 52: 72-80, 2009.
13. Chang, S., Hsyu, M.C., Cheng, H.Y. and Hsieh, S.H. Synergic co-activation of muscles in elbow flexion *via* fractional Brownian motion. *Chinese J. Physiol.* 51: 376-386, 2008.
14. Chang, S., Hsyu, M.C., Cheng, H.Y. and Hsieh, S.H. Synergic co-activation in forearm pronation. *Ann. Biomed. Eng*. 36: 2002-2018, 2008.
15. Chang, S., Hu, S.J. and Lin, W.C. Fractal dynamics and synchronization of rhythms in urodynamics of female Wistar rats. *J. Neurosci. Meth.* 139: 271-279, 2004.
16. Chang, S., Li, S.J., Chiang, M.J., Hu, S.J. and Hsyu, M.C. Fractal dimension estimation *via* spectral distribution function and its application to physiological signals. *IEEE Trans. Biomed. Eng.* 53: 1895-1898, 2007.
17. Chang, S., Li, S.J., Hu, S.J., Cheng, H.Y., Hsieh, S.H. and Cheng, C.L. Dynamic performance evaluation on the synergy of micturition in spinal cord-injured female rats under pharmacological effects. *Chinese J. Physiol.* 52: 81-92, 2009.
18. Chang, S., Mao, S.T., Hu, S.J., Lin, W.C. and Cheng, C.L. Studies of detrusor-sphincter synergia and dyssynergia during micturition in rats *via* fractional Brownian motion. *IEEE Trans. Biomed. Eng.* 47: 1066-1073, 2000.
19. Chang, S., Mao, S.T., Kuo, T.P., Hu, S.J., Lin, W.C. and Cheng, C.L. Fractal geometry in urodynamics of lower urinary tract. *Chinese J. Physiol.* 42: 25-31, 1999.
20. Cole, K.S. Membranes, Ions and Impulses. Berkeley: University of California Press, 1968.
21. Dan, Y. and Poo, M.M. Spike timing-dependent plasticity: From synapse to perception. *Physiol. Rev*. 86: 1033-1048, 2006.
22. d'Avella, A. and Bizzi, E. Shared and specific muscle synergies in natural motor behaviors. *Proc. Natl. Acad. Sci. U.S.A.* 102: 3076-3081, 2005.
23. d'Avella, A., Saltiel, P. and Bizzi, E. Combinations of muscle synergies in the construction of a natural motor behavior. *Nat. Neurosci.* 6: 300-308, 2003.
24. De Groat, W.C., Downie, J.W., Levin, R.M., Long Lin, A.T., Morrison, J.F.B., Nishizawa, O., Steers, W.D. and Thor, K.D. Basic neurophysiology and neuropharmacology, In: Incontinence, edited by Abrams, P., Khoury, S. and Wein, A. Plymouth, UK: Plymouth Distributors Ltd, 1999, pp. 105-155.
25. Delorme, A. and Makeig, S. EEGLAB: an open source toolbox for analysis of single-trial EEG dynamics. *J. Neurosci. Meth.* 134: 9-21, 2004.
26. Doob, J.L. Stochastic Processes. New York, Wiley, 1953.
27. Dupont, L., Gamet, D. and Perot, C. Motor unit recruitment and EMG power spectra during ramp contractions of a bifunctional muscle. *J. Electromyogr. Kinesiol*. 10: 217-224, 2000.
28. Eccles, J.C. Excitatory and inhibitory synaptic action. *Ann. N.Y. Acad. Sri.* 81: 247-264, 1959.
29. Ehtiati, T. and Kinsner, W. Multifractal characterization of electromyogram signals. In: Proceedings of the 1999 IEEE Canadian Conference on Electrical and Computer Engineering, 1999, pp. 792-796.
30. Farina, D., Merletti, R. and Enoka, R.M. The extraction of neural strategies from the surface EMG. *J. Appl. Physiol*. 96: 1486-1495, 2004.
31. Feder, J. Fractals. New York and London, Plenum Press, 1988.
32. Feng, T.P., Hou, H.C. and Lim, R.K.S. On the mechanism of the inhibition of gastric secretion by fat. *Chinese J. Physiol*. 3: 371, 1929.
33. Frysinger, R.C., Bourbonnais, D., Kalaska, J.F. and Smith, A.M. Cerebellar cortical activity during antagonist co-contraction and reciprocal inhibition of forearm muscles. *J. Neurophysiol*. 51: 32-49, 1984.
34. Gaskell, W.H. The Involuntary Nervous System. London, Longmans: Green and Co., 1916.
35. Gielen, C.C. and van Zuylen, E.J. Coordinations of arm muscles during flexion and supination: Application of the tensor analysis approach. *Neuroscience* 17: 527-539, 1986.
36. Gitter, J.A. and Czerniecki, M.J. Fractal analysis of the electromyographic interference pattern. *J. Neurosci. Meth.* 58: 103-108, 1995.
37. Glass, L. Synchronization and rhythmic processes in physiology. *Nature* 410: 277-284, 2001.
38. Glass, L. and Mackey, M.C. From Clocks to Chaos: The Rhythms of Life. Princeton, N.J.: Princeton University Press, 1988.
39. Goldberger, A.L., Amaral, L.A.N., Hausdorff, J.M., Ivanov, P.C., Peng, C.K. and Staley, H.E. Fractal dynamics in physiology: alternations with disease and aging. *Proc. Natl. Acad. Sci. U.S.A.* 99: 2466-2472, 2002.
40. Gupta, V., Suryanarayanan, S. and Reddy, N.P. Fractal analysis of surface EMG signals from the biceps. *Int. J. Med. Inform*. 45: 185-192, 1997.
41. Hodgkin, A.L. and Huxley, A.F. A quantitative description of membrane current and its application to conduction and excitation in nerve. *J. Physiol.* 117: 500-544, 1952.
42. Hwang, I.S. and Abraham, L.D. Quantitative EMG analysis to investigate synergistic coactivation of ankle and knee muscles during isokinetic ankle movement. Part 2: time frequency analysis. *J. Electromyogr. Kinesiol*. 11: 327-335, 2001.
43. Katok, A. and Hasselblatt, B. Introduction to the Modern Theory of Dynamical Systems. Cambridge University Press, 1995.
44. Langley, J.N. The Autonomic Nervous System. England, Cambridge: Heftier & Sons, 1921.
45. Langworhty, O.R., Kolb, L.C. and Lewis, L.G. Physiology of Micturition. Baltimore: The Williams & Wilkins Company, 1940.
46. Ling, G.N. A Revolution in the Physiology of the Living Cell, Malabar, Florida: Krieger Publishing Company, 1992.

47. Liu, A.C. On the nature of rhythm and the formation of waves of contractions in the motillty of plain muscle hollow organs. *Chinese J. Physiol*. 18: 3-7, 1960.
48. Liu, S.C. and Chang, S. Dimension estimation of discrete-time fractional Brownian motion with applications to image texture classification. *IEEE Trans. Image Process*. 6: 1176-1184, 1997.
49. Mandelbrot, B.B. The Fractal Geometry of Nature. San Francisco: Freeman, 1982.
50. Nicholls, J.G., Martin, A.R., Wallace, B.G. and Fuchs, P.A. From Neuron to Brain: A Cellular and Molecular Approach to the Function of the Nervous System. Fourth Edition, Sinauer Associates, 2001.
51. Paley, R.E.A.C. and Wiener, N. Fourier Transforms in the Complex Domain. American Mathematical Society, Providence, R. I., 1934.
52. Sacks, O. Awakenings. Vintage Books, 1990.
53. Sacks, O. Migraine. Vintage Books, 1992.
54. Sacks, O. Musicophilia: Tales of Music and the Brain. Vintage Books, 2008.
55. Sharpey-Schäfer, E.A. Textbook of Physiology. Vols. 1 & 2. Y. J. Pentland, 1898 & 1900.
56. Shefchyk, S.J. Sacral spinal interneurones and the control of urinary bladder and urethral striated sphincter muscle function. *J. Physiol*. 533: 57-63, 2001.
57. Sherrington, C.S. The Integrative Action of the Nervous System. London, Cambridge Univ. Press, 1906.
58. Standring, S. Gray's Anatomy. New York, Churchill Livingstone, 2005.
59. Winfree, A.T. The Geometry of Biological Time. Second Edition, Springer-Verlag, 2001.
60. Winfree, A.T. When Time Breaks Down. Princeton University Press, Princeton, N.J., 1987.